Journal of Zhejiang University-SCIENCE A (Applied Physics & Engineering)
ISSN 1673-565X (Print); ISSN 1862-1775 (Online)
www.zju.edu.cn/jzus; www.springerlink.com
E-mail: jzus@zju.edu.cn

Characteristics of orifices for modeling nonlinear power take-off in wave-flume tests of oscillating water column devices*

Fang HE[1], Zhenhua HUANG[†‡2]

([1]*Ocean College, Zhejiang University, Hangzhou 310058, China*)

([2]*Department of Ocean and Resources Engineering, School of Ocean and Earth Science and Technology, University of Hawaii at Manoa, Honolulu, Hawaii 96822, USA*)

[†]E-mail: zhenhua@hawaii.edu

Received Dec. 8, 2016; Revision accepted Mar. 1, 2017; Crosschecked Apr. 11, 2017

Abstract: Oscillating water column (OWC) devices for wave power extraction are appealing, but are still in need of research. In this study, a series of wave-flume experiments was conducted to examine the hydrodynamic performance of a rectangular OWC device fixed in regular waves. Two types of orifices, slot orifices and circular orifices, were used to simulate the nonlinear power take-off (PTO) mechanism, and the effects of orifice geometry were examined. A two-point measurement method was proposed to reconstruct the instantaneous spatial profile of the water surface inside the OWC chamber for reducing bias in the measured wave power extraction efficiency. The flow characteristics of PTO were described by a quadratic loss coefficient, and our experimental results showed that the quadratic loss coefficient of the slot orifices varied with wave period and slot geometry. Empirical formulas were proposed for the quadratic loss coefficients of the two types of orifices. The ability to determine the quadratic loss coefficient of an orifice will allow us to design orifices for small-scale tests and calculate the power extraction using only pressure measurement. Our results also suggested that the pressure coefficient should be more reliable than the amplification coefficient as an indicator of the power extraction performance of an OWC device.

Key words: Wave power extraction; Oscillating water column (OWC); Orifice characteristics; Quadratic loss coefficient; Contraction coefficient; Hydrodynamic efficiency

http://dx.doi.org/10.1631/jzus.A1600769 **CLC number:** P743.2

1 Introduction

Marine renewable energy could potentially provide around one million jobs by 2030 and contribute about 7% of global electricity production by 2050 (Esteban and Leary, 2012). However, utilization of marine renewable energy is facing not only great opportunities but also considerable difficulties. Research and development are still needed to make marine renewable power plants economically competitive with traditional coal-burning power plants. Wave energy is one kind of marine renewable energy with a bright future and is increasingly receiving attention in more and more countries (Falcão, 2010). Wave power resources are abundant in many regions (Iglesias and Carballo, 2009; Stopa *et al*., 2011), and the capacity of a wave power plant could be potentially comparable to that of a conventional power plant (Mei *et al*., 2005). Besides large-scale power generation, utilization of wave power is also a favorable way to meet the

‡ Corresponding author

* Project supported by the National Natural Science Foundation of China (No. 51609211), the Open Foundation of State Key Laboratory of Coastal and Offshore Engineering, Dalian University of Technology, China (No. LP1606), the Fundamental Research Funds for the Central Universities of China (No. 2016QNA4034), the Open Foundation of Key Laboratory of Water-Sediment Sciences and Water Disaster Prevention of Hunan Province, China (No. 2016SS03), the AcRF Tier 2, Ministry of Education of Singapore (No. ARC7/09MOE2008-T2-070), and a Startup Grant from the University of Hawaii at Manoa, USA

ORCID: Fang HE, http://orcid.org/0000-0002-5559-6230; Zhenhua HUANG, http://orcid.org/0000-0001-6665-7230

electricity supply for islands (Fadaeenejad *et al*., 2014; Veigas and Iglesias, 2014).

Marine renewable energy sources include offshore wind energy, current energy, ocean thermal energy, and wave energy. Recently, energy harvesting based on flow-induced vibrations has also been an emerging technology for marine renewable energy capture (Dai *et al*., 2015; Rostami and Armandei, 2017). In comparison, wave energy conversion is still in its infancy and has diversified technologies (Zhang *et al*., 2012a; Zheng *et al*., 2015; Ning *et al*., 2016a). Among the wide variety of wave energy converters, oscillating water column (OWC) devices take a leading position in research and development, and are considered as the technologies that could first achieve commercialization (Heath, 2012). A typical OWC device is a hollow pneumatic chamber with a large bottom opening under the water level and an air turbine (a power take-off mechanism) above the water level for electricity generation. Air is trapped inside the pneumatic chamber above the water column; the incoming waves cause the internal water column to oscillate and force the trapped air to flow through a self-rectifying turbine, which can be either a linear Wells turbine or a nonlinear impulse turbine. The rotation of self-rectifying turbines is unidirectional regardless of the airflow direction.

To achieve commercialization, extensive studies have been conducted to better understand the performance of various OWC devices. Theoretical studies (Sarmento and Falcão, 1985; Evans and Porter, 1995) have provided us with the fundamentals to perform mathematical modeling of OWC devices. Numerical modeling, mainly based on potential flow solvers (Delauré and Lewis, 2003; Ning *et al*., 2016b) and Navier-Stokes solvers (Zhang *et al*., 2012b; Elhanafi *et al*., 2016; 2017b), has focused on the optimization of chamber geometry and/or turbine characteristics for OWC devices. In contrast to theoretical and numerical studies, experimental studies on OWC devices are constrained by the scale of laboratory facilities, time, and funding. However, physical modeling may be the most crucial path in different development stages of wave energy converters (Falcão and Henriques, 2014; Sheng *et al*., 2014; Kuo *et al*., 2015). When designing physical model tests, it is impossible to satisfy all similarity laws (geometric similarity, kinematic similarity, and dynamic similarity) in scaled-model tests. Therefore, only important similarity laws will be satisfied in small-scale tests of OWC devices. Reynolds similarity is usually ignored as a modeling rule (Falcão and Henriques, 2014). Air compressibility may affect the OWC power plant performance at full size, but not at wave-flume scale (Elhanafi *et al*., 2017a). Although the air compressibility and Reynolds similarity cannot be completely represented in small-scale laboratory tests based on Froude similarity, the results of wave-flume tests are always valuable for validating theoretical and numerical models (López *et al*., 2014). After validation, numerical tools such as Navier-Stokes solvers may be used to study full-scale models and further evaluate possible scale-related effects such as air compressibility and Reynolds number. However, it is always desirable to collect full-scale data and carry out experimental campaigns with air compressibility and Reynolds number being properly considered in order to fully validate the numerical models.

The instantaneous water surface elevation inside the OWC chamber is spatially variant and can only be regarded as uniform when the relative chamber breadth is narrow enough or the relative chamber draft is deep enough (Evans and Porter, 1995). To study OWC devices experimentally, the spatial non-uniformity of the water surface makes accurate measurement of wave power extraction a challenging task in the past. Currently, existing experimental studies on fixed OWC devices measure the water surface elevation at only one single point inside the chamber (Thiruvenkatasamy and Neelamani, 1997; Tseng *et al*., 2000; Wang *et al*., 2002; Gouaud *et al*., 2010) and ignore the spatial non-uniformity, which may cause noticeable errors in the measured extraction efficiency (Iturrioz *et al*., 2014). Due to the difficulties in accurate measurement of wave power extraction, the surface oscillation measured at one point (Tseng *et al*., 2000; Gouaud *et al*., 2010) and the fluctuation of the air pressure inside the OWC chamber (Dizadji and Sajadian, 2011; He and Huang, 2014) have been frequently used as indicators to infer the power-extraction performance, but the reliability of using these indicators to infer the extraction efficiency of a given OWC device has not been sufficiently addressed in the literature.

For wave-flume tests, the model scale is too small to fabricate a realistically-scaled mini-turbine. In fact, it is not necessary in most cases to use scaled

turbines in wave-flume tests (Sheng *et al*., 2014); what is important is to represent satisfactorily the flow characteristics of the chosen power take-off (PTO) mechanism in the experiment. An accepted practice is to simulate the PTO mechanism using an orifice, which mimics the equivalent influence of a self-rectifying turbine (through the relationship between pressure drop and flow rate) on the wave motion. The power extracted by the orifice is the so-called 'pneumatic power' in the literature. In most previous experiments, slot or circular orifices were usually used to model the flow characteristics of PTO, but the flow characteristics of the orifices used in these existing studies have not been systematically studied. Sarmento (1992) made use of unidirectional flows in a wind tunnel to test the airflow-pressure relationship for the PTO models used in his experiments; however, the airflows through a PTO device are actually oscillatory, not unidirectional. López *et al*. (2014) used three types of slot orifices to simulate PTOs in their experiments and reported the average damping coefficient for each slot. To the best knowledge of the authors, there is still a lack of understanding about the characteristics of the orifices used in laboratory tests to model the nonlinear PTO mechanism. Without reliable experimental results on the flow characteristics of PTO, a numerical model can only treat the parameter used to describe the PTO characteristics as a fitting parameter, to be determined by comparing theory with the experiment (Wang *et al*., 2002).

Some previous experimental studies focused on the importance of OWC chamber geometry, and thus the shape and size of the orifice used to model the PTO were simply fixed when studying the hydrodynamic performance of the OWC devices under typical wave conditions (Wang *et al*., 2002; Vijayakrishna Rapaka *et al*., 2004; Morris-Thomas *et al*., 2007; He *et al*., 2012; 2013). However, a systematic optimization of the OWC devices involves both the OWC chamber geometry and the flow characteristics of PTO (Evans and Porter, 1995; López *et al*., 2014). With different PTO characteristics, the same OWC chamber could behave differently. By varying the geometry of the orifices used in small-scale tests, the flow characteristics of the PTO can be altered. Even though some experimental studies examined the hydrodynamic performance of the OWC devices using different orifices to model different flow characteristics of PTO (Thiruvenkatasamy and Neelamani, 1997; He and Huang, 2014; López *et al*., 2014; He *et al*., 2016), key factors that affect the flow characteristics of PTO have not yet been sufficiently addressed. Understanding the key factors that affect the flow characteristics of PTO is important for selecting the shape and size of an orifice for model tests.

The main objectives of this study are to: (i) introduce a method to correct the measurement bias related to the non-uniformity in the surface elevation inside the OWC chamber; (ii) provide a predictive formula for quantifying the flow characteristics of the orifices used to model PTO in small-scale OWC tests. In this study, the main objectives are achieved through a series of wave-flume experiments on the performance of a rectangular OWC device fixed in regular waves. We will use six different orifices, including two shapes and three opening ratios, to model the nonlinear PTO, so that effects of the orifice shape and opening ratio can be examined. Since the water surface elevation inside the OWC chamber can be regarded as an internal partial standing wave pattern (Evans and Porter, 1995), a two-point measurement allows us to reconstruct the instantaneous spatial profile of the water surface elevation inside the chamber and remove the measurement error related to the spatial non-uniformity (He and Huang, 2016). The experimental results will be used to provide predictive formulas for quantifying the flow characteristics of PTO for both slot and circular orifices.

2 Experimental procedures and data analysis

2.1 Physical model

The OWC models were made of 10-mm thick Perspex sheets. The front and rear walls of the OWC chamber were symmetric, and the bottom of the model was fully opened. The internal geometry of the OWC chamber was fixed at 0.53 m×0.4 m×0.4 m. The breadth B was 0.4 m, which was in the direction of wave propagation. The OWC model was designed to occupy the entire width of the wave flume so that the problem is two-dimensional. A small orifice in the top cover of the OWC chamber was used to achieve the nonlinear PTO. The orifice took the form of either a narrow slot or a circular hole. Fig. 1 shows the

geometric details of the two types of OWC models used in the present experiment: one with slot type orifice and the other with circular type orifice.

The opening ratio of the orifice α is defined as the opening area of orifice A_o divided by the cross-sectional area of OWC chamber A_c. Three opening ratios (0.625%, 1.25%, and 1.875%) were tested for each type of orifice. The three breadths of slot orifices B_o were 2.5 mm, 5.0 mm, and 7.5 mm, and the three diameters of circular orifices D_o were 41.0 mm, 58.0 mm, and 71.0 mm. The thickness of the orifice δ equaled the thickness of Perspex sheet, which was 10 mm. A target scale factor of 1:25 was used to design the model according to Froude similarity. Details of the geometric parameters of the two OWC models are summarized in Table 1.

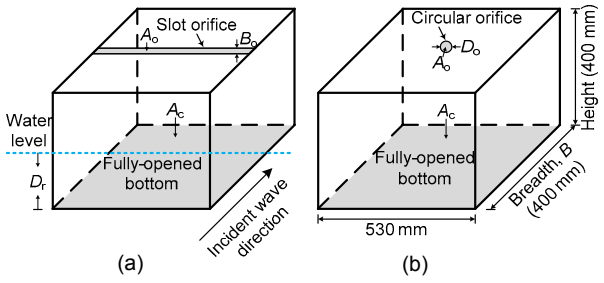

Fig. 1 Sketches of the two OWC models used in the experiments: (a) using a slot orifice to model the PTO; (b) using a circular orifice to model the PTO

Table 1 Geometric parameters of the OWC model and the test conditions

Parameter	Value
OWC model breadth, B (m)	0.4
OWC model height (m)	0.4
OWC model draft, D_r (m)	0.10, 0.15, 0.20
Breadth B_o of slot orifice (mm)	2.5 (α=0.625%), 5.0 (α=1.25%), 7.5 (α=1.875%)
Diameter D_o of circular orifice (mm)	41.0 (α=0.625%), 58.0 (α=1.25%), 71.0 (α=1.875%)
Water depth, h (m)	0.4
Wave period, T (s)	0.9–1.6 (at 0.1-s intervals)
Incident wave height, H_i (m)	0.035
Wave length, L (m)	1.22–2.84
Relative breadth, B/L	0.141–0.327
Relative draft, D_r/h	0.25, 0.375, 0.50

2.2 Experimental set-up

A sketch of the experimental set-up is shown in Fig. 2. All experiments were conducted in a glass-walled wave flume in the Hydraulics Modeling Laboratory at Nanyang Technological University, Singapore. The dimensions of the wave flume were 32.5 m long, 0.55 m wide, and 0.6 m deep. A piston-type wave generator was installed at one end of the wave flume, and a wave-absorbing beach covered with porous mats was located at the other end to reduce wave reflection. The beach reflection coefficients were less than 0.05 for all wave conditions in the present experiment.

As shown in Fig. 2, the test section was located at the middle section of the wave flume. The OWC model was placed 12 m away from the wave generator and firmly suspended in the wave flume by several holders. Eight resistance-type wave gauges (WG1–WG8) with a resolution of 0.1 mm were used to record the instantaneous water surface elevations at various locations. Two gauges (WG1 and WG2) were mounted on the OWC model to measure the water surface elevations at two locations inside the chamber. Three gauges (WG3, WG4, and WG5) were placed in front of the OWC model to separate incident waves from reflected waves. Three other gauges (WG6, WG7, and WG8) were placed on the leeward side of the OWC model to separate the transmitted waves from the waves reflected from the wave-absorbing beach. The pressure fluctuation inside the chamber was measured by three piezoresistive pressure sensors (PS1, PS2, and PS3) mounted on the OWC model. A web camera was used to monitor the water surface elevation inside the OWC chamber. The signals of WG1, WG2, PS1, PS2, PS3, and the web camera recording were synchronized.

2.3 Test conditions

A series of experiments was conducted under regular waves at a fixed water depth h of 0.4 m. The wave periods T ranged from 0.9 s to 1.6 s at 0.1-s intervals, and the target incident wave height H_i was fixed at 0.035 m. The wave length L ranged from 1.22 m to 2.84 m; the relative breadth of the OWC model B/L varied from 0.141 to 0.327. Three drafts of the OWC model D_r were tested in the experiment:

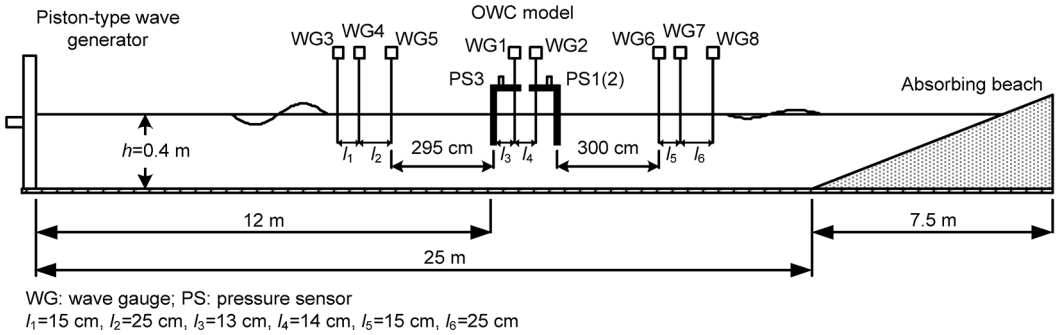

Fig. 2 A sketch of the experimental set-up (not drawn to scale)

0.1 m, 0.15 m, and 0.2 m, and thus the relative drafts D_r/h were 0.25, 0.375, and 0.50, respectively. The air leakage from the bottom opening of the OWC model could undermine the energy extraction by the PTO. In the present experiments, the drafts were deep enough to avoid the air leakage in all the test conditions. Details of the test conditions are summarized in Table 1.

2.4 Water surface elevation inside OWC chamber

Because the instantaneous water surface elevation inside the OWC chamber is spatially non-uniform and can only be regarded as uniform when the relative chamber breadth is narrow enough or the relative chamber draft is deep enough (Evans and Porter, 1995), we measured the surface elevations at two locations and constructed the water surface by performing wave separation. Fig. 3 shows sample surface elevations measured by WG1 and WG2; it can be seen that the spatial non-uniformity is noticeable, and thus the results of the previous experimental studies based on one-point measurement may be biased by the location of the wave gauge.

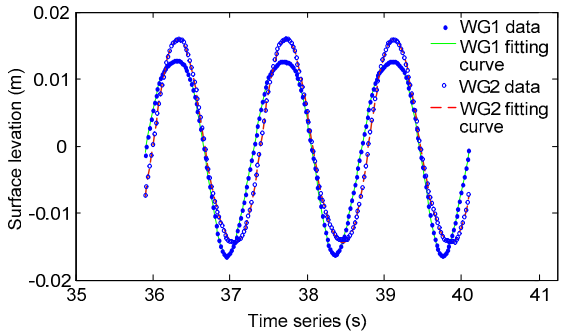

Fig. 3 A sample of the measured and fitted surface elevations for WG1 and WG2 (slot orifice, α=1.25%, D_r=10 cm, and T=1.4 s)

The water surface elevation inside the OWC chamber can be regarded as an internal partial standing wave pattern (Evans and Porter, 1995). Because the water surface was measured at two locations in this study, we were able to consider the spatial non-uniformity by performing a wave separation and reconstructing the water surface. To reconstruct the water surface inside the OWC chamber, the instantaneous water surface elevations measured by WG1 and WG2 are respectively fitted by

$$\eta_1(t)=\sum_{j=1}^{5} a_j\cos(j\omega t)+b_j\sin(j\omega t), \tag{1}$$

$$\eta_2(t)=\sum_{j=1}^{5} c_j\cos(j\omega t)+d_j\sin(j\omega t), \tag{2}$$

where ω is the angular frequency of the fundamental waves, t is the time, j is the order of harmonic waves, and a_j, b_j, c_j, and d_j are fitting parameters. Up to five harmonic wave components were included in Eqs. (1) and (2). Fig. 3 also shows a comparison between the measured surface elevations and the fitting curves. The instantaneous spatial profile of the water surface inside the OWC chamber $\eta(x, t)$ can be reconstructed by a superposition of the waves propagating in opposite directions,

$$\eta(x,t)=\sum_{j=1}^{5} A_{rj}\cos(jkx-j\omega t+\phi_{rj}) + A_{lj}\cos(jkx+j\omega t+\phi_{lj}), \tag{3}$$

where k is the wave number. The amplitudes (A_{rj}, A_{lj}) and the phases (ϕ_{rj}, ϕ_{lj}) can be determined using the measured surface elevations at the two locations

inside the chamber (i.e., $\eta_1(t)$ and $\eta_2(t)$) through a wave separation analysis by a two-point method proposed by Goda and Suzuki (1976). Fig. 4 shows an example of the reconstructed $\eta(x, t)$ using Eq. (3) for the following test conditions: slot orifice of 1.25% opening ratio, 10-cm draft of the OWC model, and 1.4 s wave period. The X-axis represents the distance from the front wall of the OWC chamber (0–0.4 m), the Y-axis represents the time (35.9–40.1 s), and the Z-axis represents the value of $\eta(x, t)$. Fig. 5 illustrates a comparison between the reconstructed surface profiles and the snapshots extracted from the video recording, which was synchronized with the wave gauges; the surface elevations measured by the two wave gauges are also included in Fig 5 for comparison. We can see that the spatial non-uniformity can be well captured by this method. For later discussion, we denote the spatially-averaged surface elevation inside the OWC chamber as

$$\bar{\eta}(t) = <\eta(x,t)>, \tag{4}$$

where $<\cdot>$ means taking a spatial average over the cross-sectional area of the OWC chamber. The spatially-averaged surface velocity can be calculated by

$$\begin{aligned}\bar{u}(t) &= <\partial\eta(x,t)/\partial t> \\ &= <\sum_{j=1}^{5} j\omega A_{tj}\cos(jkx - j\omega t + \phi_{tj} - \pi/2) \\ &\quad + j\omega A_{lj}\cos(jkx + j\omega t + \phi_{lj} + \pi/2)>,\end{aligned} \tag{5}$$

which is synchronized with the measurements of surface elevation and pressure fluctuation. Similarly, the synchronized spatially-averaged surface acceleration can be calculated by

$$\begin{aligned}\bar{a}(t) &= <\partial^2\eta(x,t)/\partial t^2> \\ &= <\sum_{j=1}^{5} j^2\omega^2 A_{tj}\cos(jkx - j\omega t + \phi_{tj} - \pi) \\ &\quad + j^2\omega^2 A_{lj}\cos(jkx + j\omega t + \phi_{lj} + \pi)>.\end{aligned} \tag{6}$$

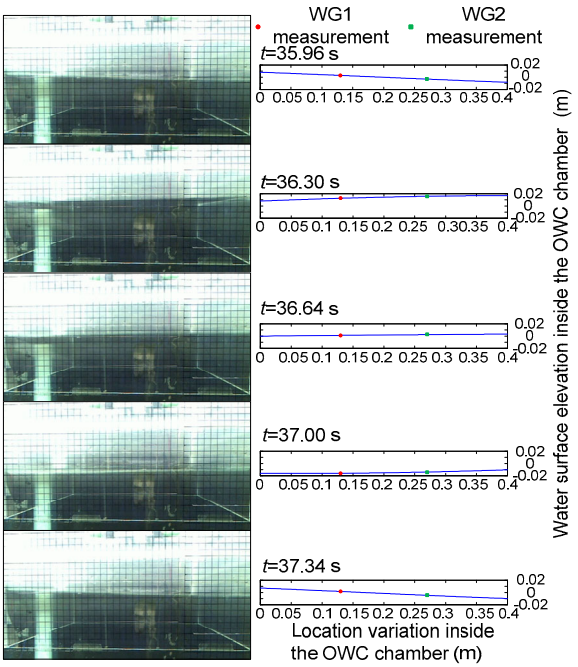

Fig. 5 Water surface elevation inside the OWC chamber during one wave period (slot orifice, α=1.25%, D_r=10 cm, and T=1.4 s. Left: snapshots extracted from the video recordings; Right: the surface elevations measured by WG1 and WG2, and the reconstructed water surface profile inside the OWC chamber. The time instants are the same for the left and right panels)

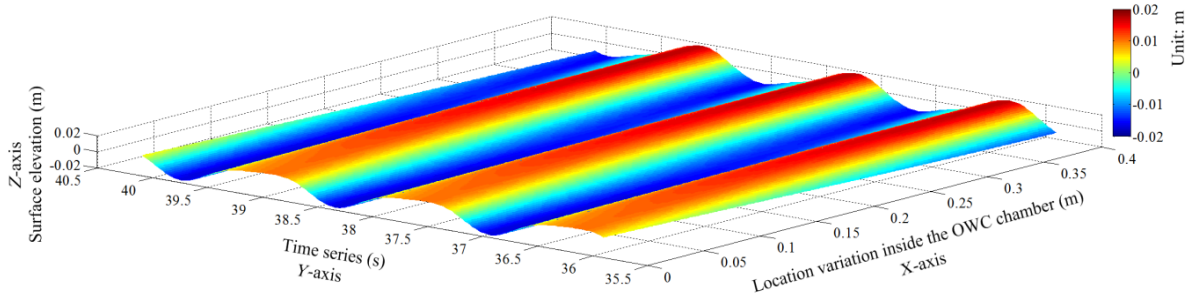

Fig. 4 Variation of the water surface elevation inside the OWC chamber with space and time (slot orifice, α=1.25%, D_r=10 cm, and T=1.4 s)

2.5 Modeling pressure drop across orifice

The orifice used to simulate nonlinear PTO is a sharp-edged orifice, and there is a pressure drop when the air flows through the orifice. Similar to the problem of slotted/perforated barriers (Mei *et al*., 1974; Huang *et al*., 2011), the pressure drop across the orifice can be modeled as

$$p(t)=\frac{\rho_{\mathrm{a}}C_{\mathrm{f}}}{2}|\overline{u}(t)|\overline{u}(t)+\rho_{\mathrm{a}}L_{\mathrm{g}}\overline{a}(t), \tag{7}$$

where $p(t)$ is the pressure fluctuation inside the OWC chamber, ρ_{a} the air density, C_{f} the quadratic loss coefficient, and L_{g} an empirical length scale. The atmospheric pressure has been set to zero in Eq. (7). The first term on the right-hand-side of Eq. (7) is the pressure drop due to drag, which causes the loss of the energy in the oscillatory air flow. The second term on the right-hand-side of Eq. (7) is an inertia term due to the acceleration of the oscillatory air flow; this term does not contribute to the loss of the energy in the oscillatory air flow. The quadratic loss coefficient C_{f} and the length scale L_{g} can be obtained by fitting Eq. (7) to the measured $p(t)$, $\overline{u}(t)$, and $\overline{a}(t)$.

In wave-flume tests of OWC devices, the air inside the OWC chamber can be considered as an incompressible fluid (Sheng *et al*., 2014). We take the air density as 1.1839 kg/m^3 in this study. For an incompressible single-phase oscillatory flow through a sharp-edged orifice, the quadratic loss coefficient can be expressed as (Mei *et al*., 2005)

$$C_{\mathrm{f}}=\left(\frac{1}{\alpha C_{\mathrm{c}}}-1\right)^2, \tag{8}$$

where C_{c} is the contraction coefficient, which describes the characteristics of the flow through the orifice.

2.6 Power extraction efficiency, amplification coefficient, and pressure coefficient

For linear waves, the incident energy flux per unit crest length can be expressed as

$$\overline{P}_{\mathrm{i}}=\frac{1}{16}\rho_{\mathrm{w}}gH_{\mathrm{i}}^2\frac{\omega}{k}\left(1+\frac{2kh}{\sinh 2kh}\right), \tag{9}$$

where ρ_{w} is the water density, and g is the gravitational acceleration. The period-averaged power extraction rate by the OWC device per unit length can be expressed as

$$\overline{P}_{\mathrm{o}}=\frac{B}{T}\int_{t_0}^{t_0+T}p(t)\overline{u}(t)\mathrm{d}t. \tag{10}$$

The power extraction efficiency ε of the OWC device can be calculated by

$$\varepsilon=\frac{\overline{P}_{\mathrm{o}}}{\overline{P}_{\mathrm{i}}}. \tag{11}$$

An amplification coefficient is defined by Eq. (12) to quantify the water surface oscillation inside the OWC chamber:

$$C_{\mathrm{a}}=\frac{\Delta_{\overline{\eta}}}{H_{\mathrm{i}}}, \tag{12}$$

where $\Delta_{\overline{\eta}}$ is the difference between the maximum and minimum values of $\overline{\eta}(t)$. The reason we choose not to use amplitudes to define this coefficient is because of the existence of higher harmonic components. Similarly, a pressure coefficient can be defined by Eq. (13) to quantify the pressure fluctuation inside the OWC chamber:

$$C_p=\frac{\Delta_p}{\rho_{\mathrm{w}}gH_{\mathrm{i}}}, \tag{13}$$

where Δ_p is the difference between the maximum and minimum values of $p(t)$ inside the chamber.

3 Results and discussion

3.1 Orifice characteristics for modeling nonlinear PTO

The ratio of the drag term to the inertia term in Eq. (7) has the following order of magnitude:

$$\beta=\frac{C_{\mathrm{f}}\Delta_{\overline{u}^2}/2}{L_{\mathrm{g}}\Delta_{\overline{a}}}, \tag{14}$$

where Δ_{u^2} is the difference between the maximum and minimum values of $|\bar{u}(t)|\bar{u}(t)$, and $\Delta_{\bar{a}}$ is the difference between the maximum and minimum values of $\bar{a}(t)$. Our data analysis showed that β ranged from 11.1 to 142.4 for the conditions tested in this study, which is consistent with the conclusions of Mei *et al*. (1974) and Huang (2007) that the inertia term in Eq. (7) was not important and could be safely dropped in most practical cases. We will use Eq. (15) to fit the measured pressure to obtain the quadratic loss coefficient C_f:

$$p(t)=\frac{\rho_a C_f}{2}|\bar{u}(t)|\bar{u}(t). \tag{15}$$

The contraction coefficient C_c can be calculated from Eq. (8); therefore, we can obtain the contraction coefficients for our orifices from the measured quadratic loss coefficient C_f.

For sharp-edged orifices, the contraction coefficient C_c depends mainly on the orifice geometry, which can be described by the relative thickness δ/D_h, where D_h is the hydraulic diameter of the orifice. The hydraulic diameter of the orifice D_h equals $4A_o/X_o$, where X_o is the orifice perimeter. In the present experiments, with the opening ratios of 0.625%, 1.25%, and 1.875%, the corresponding relative thicknesses are δ/D_h=2.01, 1.01, and 0.68 for the slot orifices, and are δ/D_h=0.24, 0.17, and 0.14 for the circular orifices. With the same opening ratio, the relative thicknesses δ/D_h can be quite different for various orifice shapes. The difference in the relative thickness δ/D_h between a slot and a circular orifice with the same opening ratio suggests the use of δ/D_h to classify these two types of orifices.

For slot orifices, the contraction coefficient may have a dependence on the relative thickness and wave period. A dimensionless period T^* defined by Eq. (16) is introduced to correlate the measured C_c as

$$T^*=\frac{T}{\sqrt{\delta/g}}. \tag{16}$$

The measured C_c for all three drafts of the OWC model tested in the experiments (D_r/h=0.25, 0.375, and 0.50) are shown in Fig. 6 as a function of T^*. Our results revealed a negligible influence of the draft on C_c; this is expected since C_c describes the flow characteristics of an orifice in an oscillatory flow, not motion of the water column inside the OWC chamber. Therefore, in Fig. 6 the values of C_c for different drafts but the same opening ratio are represented using the same symbol. Fig. 6a shows that C_c for slot orifices varies from 0.63 to 0.80, and increases with increasing wave period. It is interesting to note that it is the medium opening ratio (1.25%), not the smallest ratio (0.625%) or the largest ratio (1.875%), that gives the largest C_c for all wave periods examined in this study.

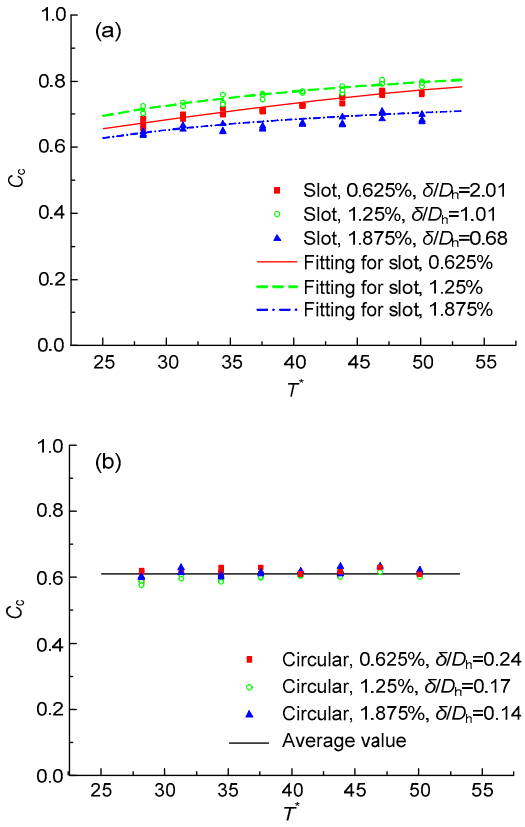

Fig. 6 Variations of contraction coefficient C_c with dimensionless wave period T^* for slot orifices (a) and circular orifices (b)

For the slot orifices, we found that the following empirical formula for contraction coefficient C_c could fit our data well:

$$C_c=\tanh\left(\frac{\pi}{2}\frac{\delta}{D_h}\right)-0.4\tanh\left(\frac{5\pi}{T^*}\frac{\delta}{D_h}\right),\quad 0.5<\delta/D_h\le 2.01. \tag{17}$$

Fig. 6a also includes a comparison between the measured C_c and the fitting curves. Since the largest δ/D_h tested in this study is 2.01, the effective range of the proposed empirical formula is $0.5<\delta/D_h\leq 2.01$. Note that the second term on the right-hand-side of Eq. (17) diminishes to zero if the airflow through the orifice is unidirectional ($T^*\to\infty$). For an oscillatory airflow, a larger relative thickness δ/D_h increases C_c through the first term on the right-hand-side of Eq. (17), but decreases C_c through the second term. This explains why it is the medium opening ratio (1.25%) that gives the largest C_c for all the wave periods examined in this study.

For circular orifices, our results showed that the dependence of C_c on both relative thickness and wave period was very weak, and C_c varied in a narrow range between 0.59 and 0.63. Therefore, an average value of C_c=0.61 can be taken to approximate C_c, as shown in Fig. 6b; this is consistent with the following well-known Chisholm expression (Fossa and Guglielmini, 2002):

$$C_c=\frac{1}{0.639(1-\alpha)^{0.5}+1}. \tag{18}$$

For the three circular orifices with opening ratio α=0.625%, 1.25%, and 1.875%, Eq. (18) gives C_c=0.6109, 0.6116, and 0.6124, respectively. Since the opening ratio α is normally small for OWC devices, the empirical value of the contraction coefficient C_c for thin-walled orifices is taken as

$$C_c=0.61, \quad \delta/D_h<0.5. \tag{19}$$

Unlike slot orifices where C_c has a strong dependence on both the relative thickness and wave period, the measured C_c for circular orifices is almost constant.

For either a slot orifice or a circular orifice, the quadratic loss coefficient C_f can be directly related to the orifice geometry using Eq. (17) or (19) into Eq. (8). We can achieve the desired PTO in model tests by choosing appropriate thickness and opening size. The quadratic loss coefficients calculated using Eqs. (8), (17), and (19) for the orifices examined in this study are summarized in Table 2. An explanation for why a slot orifice and a circular orifice with the same opening ratio behave differently is given here. If $\delta/D_h<0.5$, an orifice can be classified as a thin-walled orifice; if $\delta/D_h>0.5$, thick wall behavior takes place (Fossa and Guglielmini, 2002). Therefore, the three circular orifices are thin-walled, but the three slot orifices can no longer be considered as thin-walled. The airflow through a thin-walled orifice contracts to a vena contracta outside the orifice, and thus the flow is rarely affected by the thickness of orifice; however, if thick wall behavior takes place, the airflow begins to expand downstream of the vena contracta within the orifice, and thus the flow can feel the thickness of the orifice (Finnemore and Franzini, 2002). This explains why the opening ratio has a noticeable influence on the measured C_c for slot orifices, but negligible influence on the measured C_c for circular orifices. For a unidirectional airflow, a larger C_c occurs for a thicker orifice, and C_c eventually approaches unity with increasing δ/D_h. However, the airflow through the orifice is oscillatory, not unidirectional. The oscillation of the airflow through the orifice may influence the flow contraction, and consequently affect the value of C_c. Again, the oscillatory effect is noticeable for slot orifices, but negligible for circular orifices.

Our results showed that for the same opening ratio the orifice shape could also influence the power extraction of the OWC device. For example, the power extraction efficiency is 0.35 for the circular orifice at B/L=0.235 with 10-cm draft and 1.25% opening ratio, while the power extraction efficiency is reduced to 0.31 for the slot orifice at the same test condition.

In terms of C_f, the period-averaged power extraction rate by the OWC device per unit length, defined in Eq. (10), can be written as

$$\overline{P}_o=\frac{B}{T}\int_{t_0}^{t_0+T}\sqrt{\frac{2|p(t)|^3}{\rho_a C_f}}\mathrm{d}t. \tag{20}$$

Using our empirical expressions for the quadratic loss coefficients C_f of slot and circular orifices, one should be able to accurately calculate the power extraction by only measuring the air pressure inside the chamber. Fig. 7 shows a comparison between the measured and calculated values of ε for both the slot and circular orifices. The measured ε was obtained by directly measuring the water surface elevations at two

Table 2 Quadratic loss coefficients C_f for slot and circular orifices

T^*	C_f					
	Slot orifice			Circular orifice		
	α=0.625%	α=1.25%	α=1.875%	α=0.625%	α=1.25%	α=1.875%
28.17	56001	12279	6694	68275	16938	7470
31.30	53258	11706	6422	68275	16938	7470
34.44	50819	11246	6206	68275	16938	7470
37.57	48672	10869	6032	68275	16938	7470
40.70	46791	10556	5888	68275	16938	7470
43.83	45143	10293	5767	68275	16938	7470
46.96	43696	10069	5665	68275	16938	7470
50.09	42422	9876	5577	68275	16938	7470

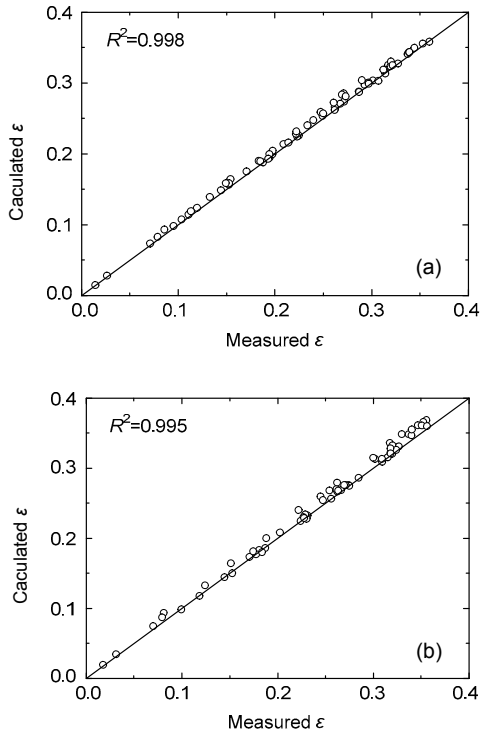

Fig. 7 A comparison of the measured and calculated ε for slot orifices (a) and circular orifices (b)

points and the pressure inside the OWC chamber; the calculated ε was obtained by measuring only the pressure inside the OWC chamber and using Eq. (20). It can be seen that the correlations between the measured and calculated values of ε were very good for both the slot and circular orifices. For illustration purposes, a comparison of the measured and calculated ε as functions of B/L is shown in Fig. A1 in Appendix A for the slot orifice of 1.25% opening ratio and 10-cm draft.

We remark that the quadratic loss coefficient describes the characteristics of the orifice controlled by the air flowing through the orifice as a throttling process between inside and outside the OWC chamber, and it is regardless of the air compressibility inside the chamber. Therefore, the quadratic loss coefficient obtained based on incompressible airflow in small-scale tests is not expected to be affected by air compressibility due to the chamber size.

3.2 Measurement bias associated with one-point measurement method

One-point measurement of the water surface elevation inside the OWC chamber was frequently used in previous work (Thiruvenkatasamy and Neelamani, 1997; Tseng *et al*., 2000; Wang *et al*., 2002; Gouaud *et al*., 2010). To illustrate the measurement bias associated with the one-point measurement method, Table 3 shows an example of the amplification coefficient calculated by spatially-averaged $\overline{\eta}(t)$, WG1-alone measured $\eta_1(t)$, and WG2-alone measured $\eta_2(t)$. It can be seen from Table 3 that large bias may occur if one measures the surface elevation at one point and uses it to describe the oscillation of the water surface inside the OWC chamber; this is especially true for the larger relative breadth of the OWC model (B/L). It can also be seen that the amplification coefficients obtained using WG1 and WG2 are different, suggesting a measurement bias exists due to the spatial non-uniformity.

Fig. 8 shows a comparison between the extraction efficiency obtained by the one-point measurement method and that obtained by the two-point measurement method. It can be seen that one-point

measurement either overestimates or underestimates the power extraction efficiency in most cases. The measured power extraction based on one-point measurement may not be accurate enough because of spatial non-uniformity. For illustration purposes, a comparison of the measured ε using the spatial averaging method, WG1-alone, and WG2-alone is provided in Fig. A2 as functions of B/L in Appendix A for the slot orifice of 1.25% opening ratio and 10-cm draft.

Table 3 Example of amplification coefficient C_a calculated using the spatially-averaged method, WG1-alone measurement, and WG2-alone measurement (slot orifice, α=1.25%, and D_r=10 cm)

B/L	C_a $(\Delta_{\bar{\eta}}/H_i)$	C_{a1} (Δ_{η_1}/H_i)	Relative bias (%)[a]	C_{a2} (Δ_{η_2}/H_i)	Relative bias (%)[b]
0.327	0.591	0.554	6.29	0.766	29.66
0.274	0.745	0.741	0.65	0.904	21.27
0.235	0.787	0.793	0.74	0.893	13.54
0.207	0.860	0.894	3.92	0.923	7.31
0.185	0.868	0.888	2.32	0.970	11.73
0.167	0.884	0.906	2.56	0.940	6.32
0.153	0.895	0.893	0.24	0.965	7.83
0.141	0.956	0.961	0.57	1.005	5.12

[a] Relative bias=100%× $|\Delta_{\eta_1}-\Delta_{\bar{\eta}}|/\Delta_{\bar{\eta}}$; [b] Relative bias=100%× $|\Delta_{\eta_2}-\Delta_{\bar{\eta}}|/\Delta_{\bar{\eta}}$

3.3 Comments on OWC performance and performance indicators

Because of the difficulties in directly measuring the wave power extraction, the amplification coefficient calculated by one-point measurement (Tseng *et al*., 2000; Gouaud *et al*., 2010) or pressure coefficient (He *et al*., 2013; He and Huang, 2014) were usually used as indicators to discuss the power extraction performance of OWC devices in previous work.

To evaluate the reliability of these indicators, Fig. 9 shows power extraction efficiency ε, pressure coefficient C_p, and amplification coefficient C_a as a function of B/L for both a slot orifice and a circular orifice of the same opening ratio; the opening ratio is 1.25% and the draft of the OWC model is 10 cm. Here, the amplification coefficient C_a is obtained using the two-point measurement method to remove the one-point measurement bias. For the slot orifice, a maximum ε of 0.337 was found at B/L=0.274, while the maximum C_p of 0.211 occurred at B/L=0.235. In contrast, C_a generally increased with decreasing B/L and reached 0.956 at the minimum B/L of 0.141. The trends of C_a and ε behave quite differently; therefore, C_a is not a good performance indicator for the power extraction efficiency. Even though the general trend of C_p is similar to that of ε, C_p is still insufficient to be an indicator to represent the power extraction efficiency. The same conclusions hold for the circular orifice: both C_p and C_a cannot indicate the trend of the power extraction efficiency. Recently, Kuo *et al*. (2017) reported similar conclusions on OWC performance and performance indicators.

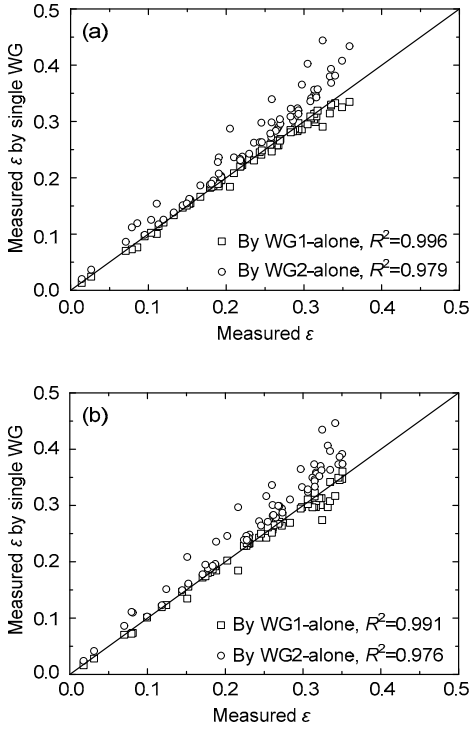

Fig. 8 A comparison of the measured ε obtained using a spatial averaging method and the measured ε obtained using a single wave gauge for slot orifices (a) and circular orifices (b)

The power extraction can be calculated using a single pressure measurement, and Eq. (20) suggests that the period-averaged power extraction by the OWC device should agree with the pressure fluctuation. Fig. 10 shows an example of the incident energy flux per unit wave crest $\overline{P}_i$ and the period-averaged power extraction by the OWC device per unit length

$\bar{P}_o$ for the circular orifice of 1.25% opening ratio and 10-cm draft. Comparing Fig. 9b with Fig. 10, it can be seen that the trend of C_a correlates to that of $\bar{P}_i$ while the trend of C_p correlates to that of $\bar{P}_o$. As an indicator of the power extraction performance of an OWC device, C_p performs more reliably than C_a, where the surface oscillation inside the chamber was mainly due to the incident energy flux and the pressure fluctuation inside the chamber can generally represent the trend of power extraction. However, the maximum power extraction and maximum power extraction efficiency do not occur at the same value of B/L. Note that the trend of ωC_a, which indicates the surface oscillation velocity inside the OWC chamber, is quite similar to that of C_p.

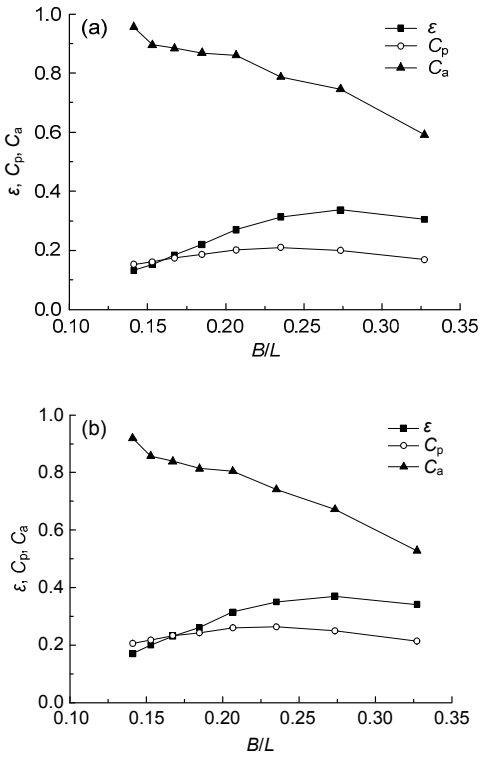

Fig. 9 Variations of extraction efficiency ε, pressure coefficient C_p, and amplification coefficient C_a with B/L for slot orifices (a) and circular orifices (b) (α=1.25% and D_r=10 cm)

Referring to Table 2, the six openings used in the experiments can simulate a wide range of quadratic loss coefficients C_f. The variations of power extraction efficiency ε, pressure coefficient C_p, and amplification coefficient C_a for the six tested openings versus B/L are shown in Fig. 11 for the OWC model with a 10-cm draft. Referring to Figs. 11b and 11c, a larger C_f generally gives a larger pressure fluctuation inside the chamber, but suppresses the surface oscillation inside the chamber. That is, the largest quadratic loss coefficient (C_f=68 275 for the circular orifice with a 0.625% opening ratio) corresponds to the largest C_p and the smallest C_a for all wave periods examined in this study. A high power extraction is the collective effect of pressure fluctuation and surface oscillation; therefore, the largest quadratic loss coefficient does not always give the highest power extraction.

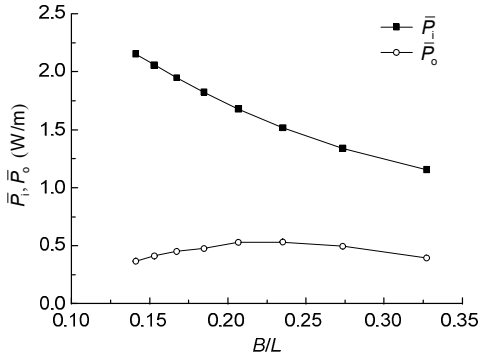

Fig. 10 Variations of incident energy flux per unit wave crest $\bar{P}_i$ and period-averaged power extraction by the OWC device per unit length $\bar{P}_o$ with B/L (circular orifice, α=1.25%, and D_r=10 cm)

Based on potential flow theory, the theoretical value of the maximum extraction efficiency is 0.5 for a suspended, 2D symmetric OWC device (Evans, 1982), but this theoretical value of 0.5 is not achievable in experiment because of the presence of viscous loss. For the 10-cm draft, the maximum overall efficiency of the OWC model was ε=0.37, which occurred at B/L=0.274 and C_f=16 938. At different wave periods (B/L), the optimal quadratic loss coefficients were different: at B/L=0.327 and 0.274 it was the circular orifice with an opening ratio of 1.25% that produced the largest ε; at B/L=0.235, 0.207, and 0.185 it was the slot orifice with an opening ratio of 0.625% that produced the largest ε; at B/L=0.167, 0.153, and 0.141 it was the circular orifice with an opening ratio

of 0.625% that produced the largest ε. Within the range of the wave periods tested in the experiments, the optimal C_f increased with increasing wave period (decreasing B/L), which is consistent with the work of Ning *et al*. (2015). Referring to Fig. 11a, too small a C_f lowered the power extraction efficiency in the entire range of B/L. The circular orifice with an opening ratio of 1.25% (a moderate C_f) gave the largest extraction efficiency and maintained the extraction efficiency high in the range of $0.235< B/L<0.327$; however, its extraction efficiency dropped significantly with decreasing B/L. In contrast, the extraction efficiency remained high when the quadratic loss coefficient was large.

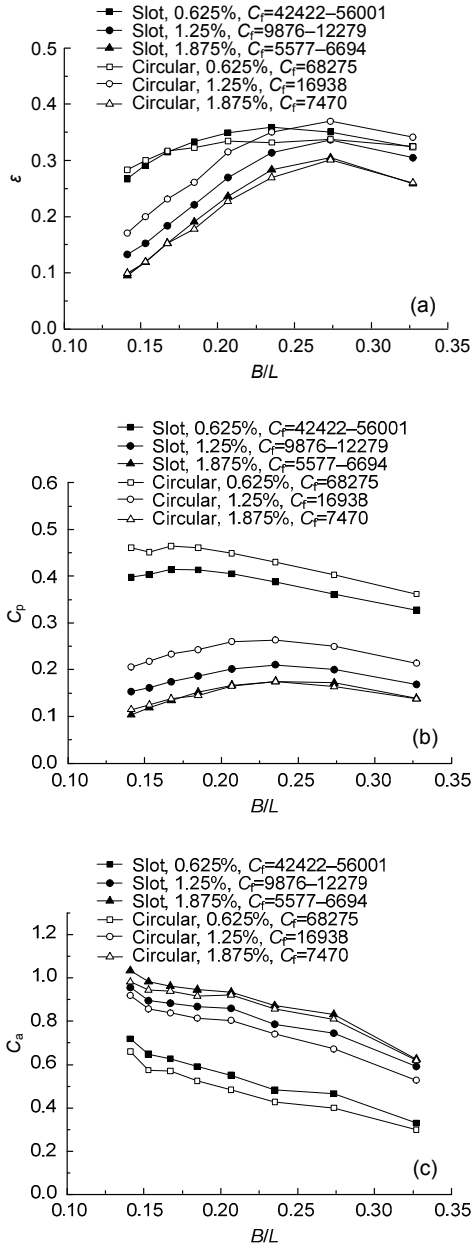

Fig. 11 Variations of extraction efficiency ε (a), pressure coefficient C_p (b), and amplification coefficient C_a (c) with B/L for D_r=10 cm

3.4 Comments on measurement of power extraction for non-rectangular OWC or oblique wave incidence

The spatially non-uniform feature of the water column inside the OWC chamber makes the accurate measurement of power extraction a challenging task, especially for non-rectangular OWC chambers or oblique wave incidence. Using our empirical formulas for the quadratic loss coefficients, which were obtained using the two-point measurement method and a reconstruction of the water surface elevation inside the OWC chamber, we can now easily measure the power extraction for non-rectangular OWC chambers or oblique wave incidence. Since the quadratic loss coefficient is not affected by the shape of the OWC or the incident angle of the waves, we can simply measure the air pressure inside the OWC chamber at one location, calculate the quadratic loss coefficient using our empirical formulas for C_f, and obtain the power extraction using Eq. (20).

4 Conclusions

In this study, a series of wave-flume experiments was conducted to examine the hydrodynamic performance of a suspended OWC device fixed in regular waves. Since the water surface elevation inside the OWC chamber is spatially non-uniform and difficult to measure accurately, this study employed a two-point measurement method, which allows us to reconstruct the instantaneous spatial profile of the water surface elevation inside the OWC chamber and remove the measurement bias associated with the one-point measurement method. It has been demonstrated that the spatial non-uniformity can be well captured by this method. To examine the effects of the orifice shape and opening ratio on the flow characteristics of PTO, six orifices, including two shapes and three opening ratios, were examined in this study. Our

results showed that the effects of both the relative thickness and oscillatory airflow were negligible for circular orifices (which can be considered as thin-walled), but noticeable for slot orifices (which can no longer be considered as thin-walled). Empirical formulas for quadratic loss coefficient were proposed, which allow us to (i) design orifices for laboratory tests of OWC devices, and (ii) accurately measure the power extraction of various OWC devices by measuring only air pressure in the OWC chamber. Our results also showed that the pressure coefficient was more reliable than the amplification coefficient as an indicator of the power extraction performance of an OWC device.

References

Dai, H.L., Abdelkefi, A., Javed, U., *et al*., 2015. Modeling and performance of electromagnetic energy harvesting from galloping oscillations. *Smart Materials and Structures*, **24**(4):045012. http://dx.doi.org/10.1088/0964-1726/24/4/045012

Delauré, Y.M.C., Lewis, A., 2003. 3D hydrodynamic modelling of fixed oscillating water column wave power plant by a boundary element methods. *Ocean Engineering*, **30**(3):309-330. http://dx.doi.org/10.1016/S0029-8018(02)00032-X

Dizadji, N., Sajadian, S.E., 2011. Modeling and optimization of the chamber of OWC system. *Energy*, **36**(5):2360-2366. http://dx.doi.org/10.1016/j.energy.2011.01.010

Elhanafi, A., Fleming, A., Macfarlane, G., *et al*., 2016. Numerical energy balance analysis for an onshore oscillating water column–wave energy converter. *Energy*, **116**:539-557. http://dx.doi.org/10.1016/j.energy.2016.09.118

Elhanafi, A., Macfarlane, G., Fleming, A., *et al*., 2017a. Scaling and air compressibility effects on a three-dimensional offshore stationary OWC wave energy converter. *Applied Energy*, **189**:1-20. http://dx.doi.org/10.1016/j.apenergy.2016.11.095

Elhanafi, A., Fleming, A., Macfarlane, G., *et al*., 2017b. Underwater geometrical impact on the hydrodynamic performance of an offshore oscillating water column–wave energy converter. *Renewable Energy*, **105**:209-231. http://dx.doi.org/10.1016/j.renene.2016.12.039

Esteban, M., Leary, D., 2012. Current developments and future prospects of offshore wind and ocean energy. *Applied Energy*, **90**(1):128-136. http://dx.doi.org/10.1016/j.apenergy.2011.06.011

Evans, D.V., 1982. Wave-power absorption by systems of oscillating surface pressure distribution. *Journal of Fluid Mechanics*, **114**:481-499. http://dx.doi.org/10.1017/S0022112082000263

Evans, D.V., Porter, R., 1995. Hydrodynamic characteristics of an oscillating water column device. *Applied Ocean Research*, **17**(3):155-164. http://dx.doi.org/10.1016/0141-1187(95)00008-9

Fadaeenejad, M., Shamsipour, R., Rokni, S.D., *et al*., 2014. New approaches in harnessing wave energy: with special attention to small islands. *Renewable and Sustainable Energy Reviews*, **29**:345-354. http://dx.doi.org/10.1016/j.rser.2013.08.077

Falcão, A.F.O., 2010. Wave energy utilization: a review of the technologies. *Renewable and Sustainable Energy Reviews*, **14**(3):899-918. http://dx.doi.org/10.1016/j.rser.2009.11.003

Falcão, A.F.O., Henriques, J.C.C., 2014. Model-prototype similarity of oscillating-water-column wave energy converters. *International Journal of Marine Energy*, **6**:18-34. http://dx.doi.org/10.1016/j.ijome.2014.05.002

Finnemore, E.J., Franzini, J.B., 2002. Fluid Mechanics with Engineering Applications. McGraw-Hill, Boston, USA.

Fossa, M., Guglielmini, G., 2002. Pressure drop and void fraction profiles during horizontal flow through thin and thick orifices. *Experimental Thermal and Fluid Science*, **26**(5):513-523. http://dx.doi.org/10.1016/S0894-1777(02)00156-5

Goda, Y., Suzuki, Y., 1976. Estimation of incident and reflected waves in random wave experiments. Proceedings of the 15th International Conference on Coastal Engineering, p.828-845. http://dx.doi.org/10.1061/9780872620834.048

Gouaud, F., Rey, V., Piazzola, J., *et al*., 2010. Experimental study of the hydrodynamic performance of an onshore wave power device in the presence of an underwater mound. *Coastal Engineering*, **57**(11-12):996-1005. http://dx.doi.org/10.1016/j.coastaleng.2010.06.003

He, F., Huang, Z., 2014. Hydrodynamic performance of pile-supported OWC-type structures as breakwaters: an experimental study. *Ocean Engineering*, **88**:618-626. http://dx.doi.org/10.1016/j.oceaneng.2014.04.023

He, F., Huang, Z., 2016. Using an oscillating water column structure to reduce wave reflection from a vertical wall. *Journal of Waterway, Port, Coastal, and Ocean Engineering*, **142**(2):04015021. http://dx.doi.org/10.1061/(asce)ww.1943-5460.0000320

He, F., Huang, Z., Law, A.W.K., 2012. Hydrodynamic performance of a rectangular floating breakwater with and without pneumatic chambers: an experimental study. *Ocean Engineering*, **51**:16-27. http://dx.doi.org/10.1016/j.oceaneng.2012.05.008

He, F., Huang, Z., Law, A.W.K., 2013. An experimental study of a floating breakwater with asymmetric pneumatic chambers for wave energy extraction. *Applied Energy*, **106**:222-231. http://dx.doi.org/10.1016/j.apenergy.2013.01.013

He, F., Li, M., Huang, Z., 2016. An experimental study of

pile-supported OWC-type breakwaters: energy extraction and vortex-induced energy loss. *Energies*, **9**(7):540. http://dx.doi.org/10.3390/en9070540

Heath, T.V., 2012. A review of oscillating water columns. *Philosophical Transactions of the Royal Society A: Mathematical, Physical and Engineering Sciences*, **370**(1959):235-245. http://dx.doi.org/10.1098/rsta.2011.0164

Huang, Z., 2007. Wave interaction with one or two rows of closely spaced rectangular cylinders. *Ocean Engineering*, **34**(11-12):1584-1591. http://dx.doi.org/10.1016/j.oceaneng.2006.11.002

Huang, Z., Li, Y., Liu, Y., 2011. Hydraulic performance and wave loadings of perforated/slotted coastal structures: a review. *Ocean Engineering*, **38**(10):1031-1053. http://dx.doi.org/10.1016/j.oceaneng.2011.03.002

Iglesias, G., Carballo, R., 2009. Wave energy potential along the Death Coast (Spain). *Energy*, **34**(11):1963-1975. http://dx.doi.org/10.1016/j.energy.2009.08.004

Iturrioz, A., Guanche, R., Armesto, J.A., *et al*., 2014. Time-domain modeling of a fixed detached oscillating water column towards a floating multi-chamber device. *Ocean Engineering*, **76**:65-74. http://dx.doi.org/10.1016/j.oceaneng.2013.11.023

Kuo, Y.S., Lin, C.S., Chung, C.Y., *et al*., 2015. Wave loading distribution of oscillating water column caisson breakwaters under non-breaking wave forces. *Journal of Marine Science and Technology*, **23**(1):78-87. http://dx.doi.org/10.6119/JMST-014-0114-1

Kuo, Y.S., Chung, C.Y., Hsiao, S.C., *et al*., 2017. Hydrodynamic characteristics of oscillating water column caisson breakwaters. *Renewable Energy*, **103**:439-447. http://dx.doi.org/10.1016/j.renene.2016.11.028

López, I., Pereiras, B., Castro, F., *et al*., 2014. Optimisation of turbine-induced damping for an OWC wave energy converter using a RANS-VOF numerical model. *Applied Energy*, **127**:105-114. http://dx.doi.org/10.1016/j.apenergy.2014.04.020

Mei, C.C., Liu, P.L., Ippen, A.T., 1974. Quadratic loss and scattering of long waves. *Journal of the Waterways, Harbors and Coastal Engineering Division*, **100**(3):217-239.

Mei, C.C., Stiassnie, M., Yue, D.K.P., 2005. Theory and Applications of Ocean Surface Waves. World Scientific, Singapore.

Morris-Thomas, M.T., Irvin, R.J., Thiagarajan, K.P., 2007. An investigation into the hydrodynamic efficiency of an oscillating water column. *Journal of Offshore Mechanics and Arctic Engineering*, **129**(4):273-278. http://dx.doi.org/10.1115/1.2426992

Ning, D.Z., Shi, J., Zou, Q.P., *et al*., 2015. Investigation of hydrodynamic performance of an OWC (oscillating water column) wave energy device using a fully nonlinear HOBEM (higher-order boundary element method). *Energy*, **83**:177-188. http://dx.doi.org/10.1016/j.energy.2015.02.012

Ning, D.Z., Zhao, X.L., Göteman, M., *et al*., 2016a. Hydrodynamic performance of a pile-restrained WEC-type floating breakwater: an experimental study. *Renewable Energy*, **95**:531-541. http://dx.doi.org/10.1016/j.renene.2016.04.057

Ning, D.Z., Wang, R.Q., Gou, Y., *et al*., 2016b. Numerical and experimental investigation of wave dynamics on a land-fixed OWC device. *Energy*, **115**:326-337. http://dx.doi.org/10.1016/j.energy.2016.09.001

Rostami, A.B., Armandei, M., 2017. Renewable energy harvesting by vortex-induced motions: review and benchmarking of technologies. *Renewable and Sustainable Energy Reviews*, **70**:193-214. http://dx.doi.org/10.1016/j.rser.2016.11.202

Sarmento, A.J.N.A., 1992. Wave flume experiments on two-dimensional oscillating water column wave energy devices. *Experiments in Fluids*, **12**(4):286-292. http://dx.doi.org/10.1007/BF00187307

Sarmento, A.J.N.A., Falcão, A.F.O., 1985. Wave generation by an oscillating surface-pressure and its application in wave-energy extraction. *Journal of Fluid Mechanics*, **150**:467-485. http://dx.doi.org/10.1017/S0022112085000234

Sheng, W., Alcorn, R., Lewis, T., 2014. Physical modelling of wave energy converters. *Ocean Engineering*, **84**:29-36. http://dx.doi.org/10.1016/j.oceaneng.2014.03.019

Stopa, J.E., Cheung, K.F., Chen, Y.L., 2011. Assessment of wave energy resources in Hawaii. *Renewable Energy*, **36**(2):554-567. http://dx.doi.org/10.1016/j.renene.2010.07.014

Thiruvenkatasamy, K., Neelamani, S., 1997. On the efficiency of wave energy caissons in array. *Applied Ocean Research*, **19**(1):61-72. http://dx.doi.org/10.1016/S0141-1187(97)00008-4

Tseng, R.S., Wu, R.H., Huang, C.C., 2000. Model study of a shoreline wave-power system. *Ocean Engineering*, **27**(8):801-821. http://dx.doi.org/10.1016/S0029-8018(99)00028-1

Veigas, M., Iglesias, G., 2014. Potentials of a hybrid offshore farm for the island of Fuerteventura. *Energy Conversion and Management*, **86**:300-308. http://dx.doi.org/10.1016/j.enconman.2014.05.032

Vijayakrishna Rapaka, E., Natarajan, R., Neelamani, S., 2004. Experimental investigation on the dynamic response of a moored wave energy device under regular sea waves. *Ocean Engineering*, **31**(5-6):725-743. http://dx.doi.org/10.1016/j.oceaneng.2003.09.001

Wang, D.J., Katory, M., Li, Y.S., 2002. Analytical and experimental investigation on the hydrodynamic performance of onshore wave-power devices. *Ocean Engineering*, **29**(8):871-885. http://dx.doi.org/10.1016/S0029-8018(01)00058-0

Zhang, D., Li, W., Lin, Y., *et al*., 2012a. An overview of hydraulic systems in wave energy application in China.

Renewable and Sustainable Energy Reviews, **16**(7):4522-4526.
http://dx.doi.org/10.1016/j.rser.2012.04.005

Zhang, Y., Zou, Q.P., Greaves, D., 2012b. Air–water two-phase flow modelling of hydrodynamic performance of an oscillating water column device. *Renewable Energy*, **41**:159-170.
http://dx.doi.org/10.1016/j.renene.2011.10.011

Zheng, S.M., Zhang, Y.H., Zhang, Y.L., *et al*., 2015. Numerical study on the dynamics of a two-raft wave energy conversion device. *Journal of Fluids and Structures*, **58**:271-290.
http://dx.doi.org/10.1016/j.jfluidstructs.2015.07.008

Appendix A: Comparison among different methods for determination of extraction efficiency

For illustration purposes, Fig. A1 shows a comparison between the extraction efficiency ε measured using the two-point method and the one calculated using Eq. (20). Fig. A2 shows a comparison among the values of extraction efficiency ε obtained by (i) the spatial averaging method, (ii) WG1-alone, and (iii) WG2-alone. For both figures, the experimental test conditions are: slot orifice of 1.25% opening ratio and 10-cm draft of the OWC model.

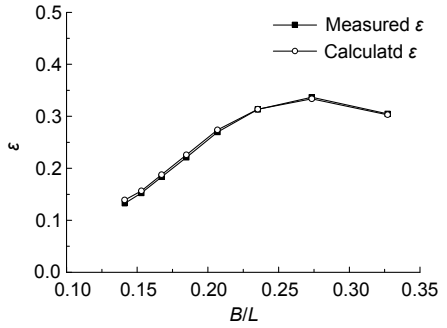

Fig. A1 A comparison between the measured and calculated extraction efficiency ε

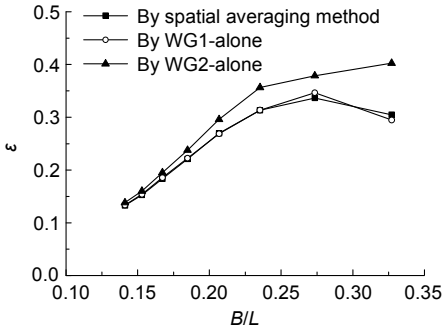

Fig. A2 A comparison among the extraction efficiency ε obtained by spatial averaging method, WG1-alone, and WG2-alone

中文概要

题　目：振荡水柱装置波浪水槽试验中用于模拟非线性能量俘获系统的孔口特性

目　的：在振荡水柱装置研究中，通常通过不同的孔口几何特征来改变能量俘获系统的特性，但其具体流动特性却鲜有报道。本文探讨孔口几何特征（形状、尺寸和开孔率等）对流动特性的影响机制，理解影响能量俘获系统特性的关键因素，研究其对振荡水柱装置水动力特性和波能提取的影响规律，并评估波能提取性能指标的有效性。

创新点：1. 提出了两点测量法来重构振荡水柱腔室内液面；2. 建立了孔口流动特性与孔口几何特征的关系式；3. 提出了仅测量腔室内气压即可获得波能提取功率的方法；4. 该方法可扩展至非二维矩形腔室及斜向波。

方　法：1. 采用不同尺寸狭缝孔和圆形孔来模拟非线性能量俘获系统；2. 通过一系列波浪水槽试验，对振荡水柱装置的水动力特性及波能的提取展开研究；3. 采用二次损耗系数和收缩系数来描述孔口往复流动特性，并构建其与孔口几何特征的关系；4. 通过两点测量法获取振荡水柱腔室内的准确信息；5. 评估压力波动系数和液面放大系数作为振荡水柱装置波能提取性能指标的有效性。

结　论：1. 两点测量法能够重建二维矩形振荡水柱腔室内液面的瞬时空间分布，消除了单点法的测量偏差；2. 孔口相对厚度及振荡气流对可被视为薄壁的圆形孔的影响可以忽略不计，但对不能视为薄壁的狭缝孔的影响显著；3. 本文提出的二次损耗系数经验公式可用于（1）通过孔口几何尺寸设计其流动特性和（2）通过仅测量腔室内气压来计算波能提取功率；4. 用作振荡水柱装置的波能提取性能指标时，压力波动系数比液面放大系数更为可靠。

关键词：波能提取；振荡水柱；孔口特性；二次损耗系数；收缩系数；水动力效率

Introducing new editorial board member:

Dr. Zhenhua HUANG obtained both his BEng and MEng in Fluid Mechanics from Tsinghua University, China. He obtained his PhD in Environmental Fluid Mechanics from the Massachusetts Institute of Technology, USA. Prior to joining the University of Hawaii at Manoa, USA in 2014, he was a faculty member first at the Hong Kong University of Science and Technology, China (2004-2006) and then at Nanyang Technological University, Singapore (2007-2013). He was a Principal Investigator of the Earth Observatory of Singapore, where he led a research group working on tsunami hydrodynamics from 2009 to 2014. He has been a member of the International Steering Committee for Asian and Pacific Coasts (APAC) since 2007. Dr. HUANG's research interests lie in the broad field of hydrodynamics and its applications in coastal and ocean engineering. His recent research activities include hydrodynamics of marine structures, wave-energy conversion, coastal sediment transport, coral reef hydrodynamics, and tsunami hydrodynamics.